Numerical Prediction of Nonequilibrium Hypersonic Flow Around Brazilian Satellite SARA

Ghislain Tchuen,
Institut Universitaire de Technologie Fotso Victor
Université de Dschang, BP. 134 Bandjoun - Cameroun

Yves Burtschell, and David E. Zeitoun
Université de provence, Polytech'Marseille-DME, 5 rue Enrico Fermi
Technopole de Chateau Gombert, 13453 Marseille Cedex 13, France

Received on 29 June, 2004. Revised version received on 15 October, 2004

Hypersonic flows past Brazilian satellite SARA at zero angle of attack in chemical and thermal nonequilibrium are investigated using an axisymmetric Navier-Stokes solver. The numerical solutions were carried out for freestream conditions equivalent to a typically re-entry trajectory with a range of Mach numbers from 10 to 25. The gas was chemically composed by seven air species $O, N, NO, O_2, N_2, NO^+, e^-$ with 24 steps chemical reactions scheme and thermically characterized by a multi-temperature model. Comparisons have been made between the present computation and the distribution of pressure coefficient and the heat transfer obtained recently with Direct Simulation Monte Carlo Method[1]. The study also points out the influence of nonequilibrium phenomena like ionization, vibrational and electronic excitation on aerothermodynamic flow parameters.

1 Introduction

Recently, Sharipov predicted by the DSMC method and for a frozen flow (without chemical reactions), the aerothermodynamic parameters which are necessary for the calculation of the ballistic trajectory of re-entry and for the creation of an adequate aerothermic protection of a small reusable ballistic Brazilian satellite SARA[1]. The atmospheric conditions used goes from the free molecular regime up to the hydrodynamic medium.

The development of the satellite re-entry into atmosphere requires accurate prediction of the thermal protection system for extremely high temperature. The vehicle flying with hypersonic velocity through the Earth's upper atmosphere. This creates a detached shock wave around the vehicle and the kinetic energy is transformed into the internal energy. Therefore, the shock layer is the site of intensive physico-chemical nonequilibrium processes such as vibrational excitation, dissociation- recombination, electronic excitation, significant ionization and radiative heating[2]. These are commonly referred as high-temperature effects which causes considerable difficulties for accurate numerical and experimental simulations of the flowfield. Successful conception of such high technology would be obtained after some knowledge of the thermochemical nonequilibrium phenomena and how they affect the performance of the vehicle.

In this study, an effort is being spent to the numerical prediction of the aerothermodynamic characteristics of satellite for very high altitude with a Knudsen number relatively suitable to the application of Navier-Stokes equations. According to the Mach number and heating effects observed, nonequilibrium chemical, vibrational and electronic modes are taken into account. The series of calculations are carried out taking into account, in a progressive way the assumptions which allow as well as possible to approach the reality of physics within the flow. The numerical simulations begin with a frozen air flow, followed by the taking into account of a chemical kinetics with 5 species in which the various couplings are included. The last step is made by an extension for conditions being able to cause significant ionization of gas (chemical kinetics with 7 species) and the electronic excitation of the species. An efficient and robust thermochemical nonequilibrium Navier-Stokes code based on Upwing technology with Riemann's solver has been developed.

The various upstream flow conditions are considered with a wide range of Mach numbers(10 up to 25). SARA is a sphere-cone and its shape is shown in Fig. 1. The nose raduis is equal to 0.27544 m. The numerical results obtained under the same conditions of simulation have been well compared with available DSMC computations[1].

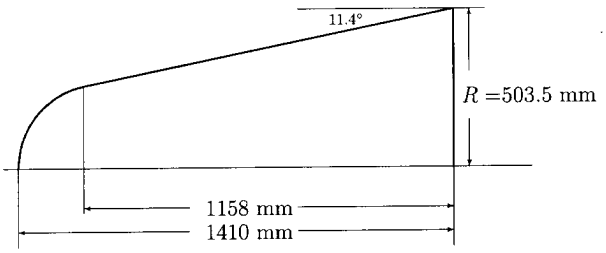

Figure 1. Shape of satellite SARA

2 Governing equations

The governing equations for a real gas are reported following the simplifications discussed by Lee[3]. The full laminar Navier-Stokes equations for two-dimensional conservation equations are written as:
The mass conservation equation for each species, s,

$$\frac{\partial \rho_s}{\partial t} + \frac{\partial \rho_s u_j}{\partial x_j} + \frac{\partial \rho_s V_s^j}{\partial x_j} = \omega_s \tag{1}$$

The momentum conservation equation in x and y directions,

$$\frac{\partial \rho u_i}{\partial t} + \frac{\partial (\rho u_i u_j + p\delta_{ij})}{\partial x_j} + \frac{\partial \tau_{ij}}{\partial x_j} = 0 \tag{2}$$

The total energy equation,

$$\frac{\partial \rho e}{\partial t} + \frac{\partial ((\rho e + p)u_j)}{\partial x_j} + \frac{\partial u_i \tau_{ij} + q_{t_j} + q_{v_m j} + q_{e_j} + \sum_s^{ns} (\rho_s h_s V_s^j)}{\partial x_j} = 0 \tag{3}$$

The conservation equation of vibrational energy for each nonequilibrium molecule,

$$\frac{\partial \rho e_{v_m}}{\partial t} + \frac{\partial (\rho e_{v_m} u_j)}{\partial x_j} + \frac{\partial (q_{v_j} + \rho_m e_{v_m} V_m^j)}{\partial x_j} = Q_{T-v_m} + Q_{v_m - v_r} + Q_{v_m - e} \tag{4}$$

The electron-electronic energy conservation equation

$$\frac{\partial \rho e_e}{\partial t} + \frac{\partial ((\rho e_e + p_e)u_j)}{\partial x_j} + \frac{\partial (q_{e_j} + \sum_s \rho_s e_{e_s} V_s^j)}{\partial x_j} = u_j \frac{\partial p_e}{\partial x_j} - Q_{v_m - e} + Q_{T-e} + Q_{el} \tag{5}$$

In these equations, the electric field due to the presence of electrons in flow is expressed as:

$$\overrightarrow{E} \simeq -\frac{1}{N_e \epsilon} \overrightarrow{\nabla} p_e \tag{6}$$

The shear stresses are modelled using the hypothesis of a newtonian fluid as:

$$\tau_{ij} = -\mu \left(\frac{\partial u_i}{\partial x_j} + \frac{\partial u_j}{x_i} \right) - \lambda \frac{\partial u_k}{\partial x_k} \delta_{ij}, \qquad \text{with} \qquad \lambda = -\frac{2}{3}\mu \tag{7}$$

The dynamic vicosity μ_s of each species is given by Blottner et al.[4] and the thermal conductivity of each species is derived from Eucken's[5]. The total viscosity and conductivity of the gas are calculated using Wilke's semi-empirical mixing rule[6].
The mass diffusion fluxes for s-species are given by Fick's law with a single diffusion coefficient D_s as:

$$\rho_s V_s^j = -\rho D_s \frac{\partial Y_s}{\partial x_j} \tag{8}$$

Where the expression of diffusion coefficient is obtained by assuming a constant Lewis number (L_e=1.2). When ionized species are included, the diffusion of ions and electrons is modeled with ambipolar diffusion as recommended in ref[7]. The heat flux (conductive, chemical, vibrational and electronic counterparts) are defined as:

$$\overrightarrow{Q} = \overrightarrow{q}_{tr} + \overrightarrow{q}_{v} + \overrightarrow{q}_{el} + \overrightarrow{q}_{chem} \tag{9}$$

with

$$\overrightarrow{q}_{tr} = -\lambda_{tr} \nabla T \qquad \overrightarrow{q}_{v} = \sum_{m=mol} -\lambda_{v,m} \nabla T_{v_m}$$
$$\overrightarrow{q}_{el} = -\lambda_{el} \nabla T_e \qquad \overrightarrow{q}_{chem} = \sum_i h_i \rho_s V_s^j \tag{10}$$

The total energy of the mixture per unit volume

$$\rho e = \sum_{s \neq e} \rho_s C^s_{v,tr} T + \frac{1}{2} \sum_s \rho_s u_s^2 + \sum_{m=1}^{NM} \rho_m e_{v_m} + \rho e_e + \sum_{s=1}^{NS} \rho_s h_s^0 \quad (11)$$

is splitted between the translational-rotational, kinetic, vibrational, electron-electronic contributions, and the latent chemical energy of the species. The total pressure is given by Dalton's law as the sum of partial pressure of each species regarded as perfect gas.

$$p = \sum_{s=1}^{NS} p_s = \sum_{s \neq e} \rho_s R_s T + \rho_e R_e T_e \quad (12)$$

3 Numerical simulations

The governing equations are integrated using an efficient and robust thermochemical nonequilibrium Navier-Stokes solver. The present code is based on the Upwing technology with exact Riemann's solver algorithm, in conjunction with a second-order MUSCL -TVD type scheme approach[8], coupled with a multi-block finite volume scheme.

The system of equations (1)-(5) can be reduced in only one as follows:

$$\frac{\partial U}{\partial t} + \frac{\partial (F_c + F_v)}{\partial x_j} = \Omega \quad (13)$$

Where U is the conservative vector, F_c the convectif flux, F_v the viscous flux and Ω the source term.

The explicit formulation which gives the variation of $U_{i,j}$ during time Δt on each cell (i, j) can be written in two dimensional axisymmetric coordinate as[9]:

$$\frac{\Delta U_{i,j}}{\Delta t} + \frac{1}{A_{i,j} r^{\alpha}_{i,j}} \sum_{k=1}^{4} F_k N_k = \alpha H_{i,j} + \Omega_{i,j} \quad (14)$$

where $\alpha = 1$ for an axisymmetry coordinate system, and $\alpha = 0$ for planar two-dimensions. This equation allows us to calculate numerically the all unknown variables in all computational domain. The exact Riemann solver and the Mimmod limiter function are used for the convective fluxes. The viscous terms are classically discretized by second-order central difference approximation. The source terms Ω are treated implicitly to relax the stiffness. The semi-implicit predictor-corrector schema can be written as:

$$Pred. : \left[I - \frac{\Delta t}{2} \frac{\partial \Omega_{i,j}}{\partial U_{i,j}} \right] \Delta U_{i,j} = -\frac{\Delta t}{2} . R^n; \quad \Delta U_{i,j} = U^{n+1/2}_{i,j} - U^n_{i,j} \quad (15)$$

$$Corr. : \left[I - \Delta t \frac{\partial \Omega_{i,j}}{\partial U_{i,j}} \right] \Delta U_{i,j} = -\Delta t . R^{n+1/2}; \quad \Delta U_{i,j} = U^{n+1}_{i,j} - U^n_{i,j} \quad (16)$$

where R^n is the residual calculated explicitly at time step n. The steady state is obtained after convergence of the unsteady formulation of the discretized equations. The algorithm is second order accurate in space and time.

The modified speed of sound which takes into account the nonequilibrium electronic is implemented in the flux splitting procedure as[10]:

$$c^2 = \gamma \left(\frac{p}{\rho} \right) + (\gamma - 1) \left(\frac{T}{T_e} - 1 \right) \frac{p_e}{\rho} \quad (17)$$

where classical frozen speed of sound is obtained when $T = T_e$.

TABLE 1. Upstream conditions for satellite SARA

Mach	10	10	20	25
Altitude, (Km)	80	75	80	80
$U_\infty, (m/s)$	2811.2	2816.45	5622.4	7028
$P_\infty, (P_a)$	0.8627	2.08393	0.8627	0.8627
$T_\infty, (^oK)$	196.65	196.65	196.65	196.65
T_{wall}/T_∞	1	1	1	1
R_e	2161.80	4000	4323.6019	5404.5024
K_n	6.87x10^{-3}	3.7143x10^{-3}	6.874x10^{-3}	6.874x10^{-3}
Grid IM	50	50	60	60
Grid JM	50	50	80	90
$\Delta x_{min}(m)$	2.5946x10^{-4}	2.5946x10^{-4}	1.0230x10^{-4}	4.6709x10^{-5}
$\Delta y_{min}(m)$	2.0522x10^{-3}	2.0522x10^{-3}	2.4606x10^{-4}	2.3025x10^{-4}

4 Results and comparisons

The conditions of simulation are defined from the following parameters:
The Mach number is given as:

$$M_a = \frac{U_\infty}{c} \tag{18}$$

where c is the speed of sound defined earlier
The Reynolds number is given as:

$$R_e = \frac{RU_\infty \rho_\infty}{\mu} \tag{19}$$

where R is the largest satellite radius as shown in Fig. 1. These two parameters allow to define the gas rarefaction which is characterized with the Knudsen number as[1]:

$$K_n = \frac{M_a}{R_e}\sqrt{\gamma\frac{\pi}{2}} \tag{20}$$

The various aerothermodynamic parameters calculated along the wall in this paper are defined as follows:
Skin friction coefficient

$$C_f = \frac{\tau_w}{\frac{1}{2}\rho_\infty U_\infty^2} \tag{21}$$

Pressure coefficient

$$C_p = \frac{P - P_\infty}{\frac{1}{2}\rho_\infty U_\infty^2} \tag{22}$$

Wall heat transfer coefficient

$$C_h = \frac{Q_w}{\frac{1}{2}\rho_\infty U_\infty^3} \tag{23}$$

Upstream conditions
The upstream conditions are chosen in order to make comparisons with Sharipov's results given in ref.[1]. In this paper the results are presented for 3 values of the Reynolds number (0,1 ; 10 and 4000) and for Mach number (5, 10, 20). The conditions used in this work are gathered in the table 1, and are extract from the abacus of the standard atmosphere[11]. The altitude of 80 km is retained because of the Reynolds number is close to 4000.

Boundary conditions
The boundary conditions are imposed along the satellite. The wall temperature is selected equal to the temperature of the upstream flow from which the various characteristics are given in the table 1. The walls are supposed chemically noncatalytic, no-slip and no-temperature jump boundary conditions are used. The freestream is hypersonic and all flow variables are known. The outflow is supersonic and therefore the zero gradient exit condition is appropriate. The influence of the temperature of wall on the variables aerothermodynamics was studied by Sharipov[1] and is not included in this study.

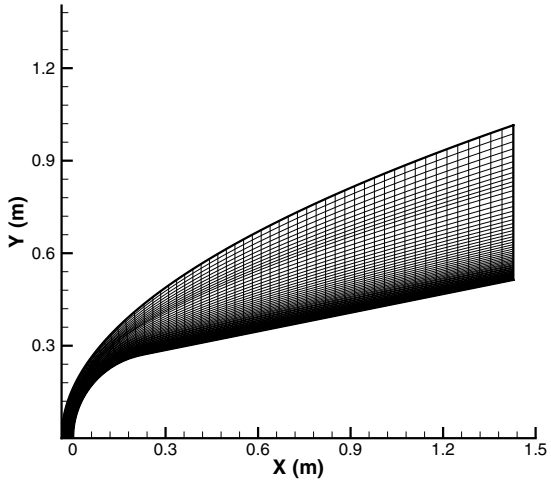

Figure 2. Numerical grid.

Figure 2 shows the geometry and grid used in the calculations. The grid point is densely distributed near the wall and near the shock standoff distance. The minimum grid spacing in x and y directions are respectively carried in the table 1. The time step is classically determined by explicit stability criteria and the Courant-Friedrichs-Lewy (CFL) number used in all computations varying from 0.01 to 0.4.

Results

Case Mach 10

Figure 3 represents the translational temperature isocontours in the flow at $R_e = 4000$. The maximum value of the temperature ratio T/T_∞ behind the shock wave is around 20 which is 30% weaker than the value predicted by Sharipov. The obtained temperature can cause only a very weak dissociation of the oxygen molecules. Consequently, chemical nonequilibrium is not taken into account in this case. The skin friction coefficient C_f, the pressure coefficient C_p and the wall heat transfer coefficient C_h are represented in Figs. 4, 5 and 6 as a function of the angle θ for two Reynolds numbers (2161.8 and 4000). The Reynolds number has a significant influence on the peak of C_f. For identical Mach numbers, the evolution of C_f strongly depends on two parameters : the radius of the satellite and the Reynolds number. One can notice that the passage of the altitude 80 to 75 km, involves a decrease of the peak of about 41.93%. The results obtained for C_p and C_h are compared in Figs. 5 and 6 with those obtained with DSMC[1]. The influence of the Reynolds number is also pointed out with an increase of 35.4% of C_h at the stagnation point. For the same values of the Reynolds number (4000), one notes a rather good agreement with Sharipov's results[1]. The numerical simulation continues with a Mach number equal to 20 in which the thermochemical nonequilibrium becomes significant.

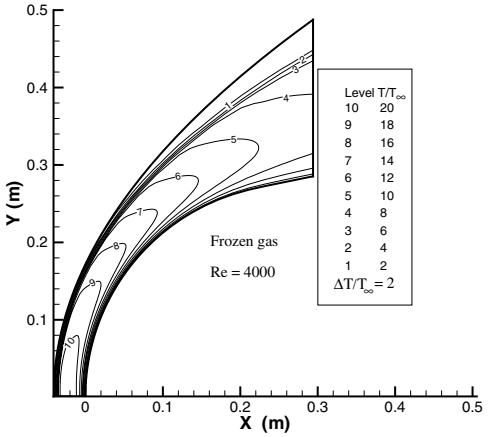

Figure 3. Isocontours of translational temperature; Mach 10.

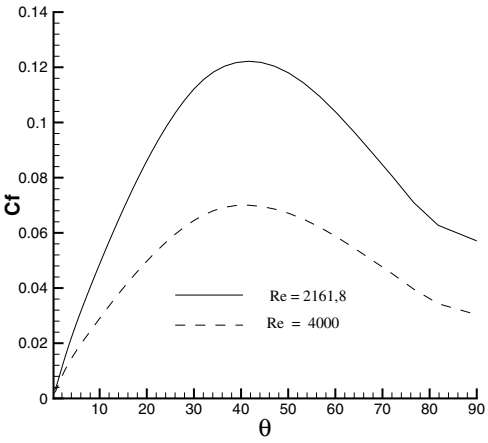

Figure 4. Friction Coefficient; Mach 10.

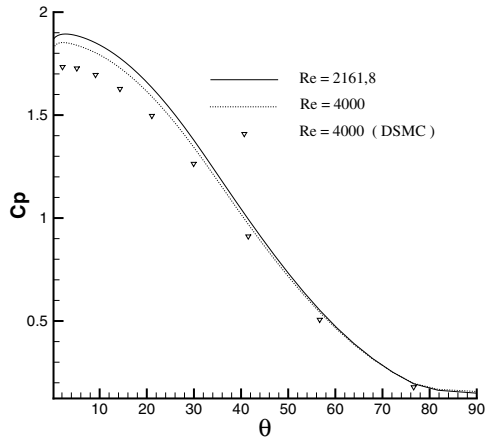

Figure 5. Comparison with the DSMC of the coefficient C_p; Mach 10.

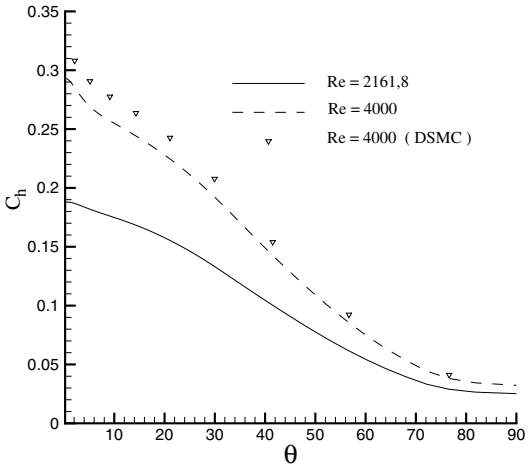

Figure 6. Comparison with the DSMC of the coefficient C_h; Mach 10.

Case Mach 20

When the velocity of the vehicle increases, more kinetic energy is absorbed by the initial air molecules and the nonequilibrium processes such as vibrational excitation, rapid dissociation- recombinaison take place in the shock layer. Consequently, the physico-chemical phenomena are simultaneously set up and are included here. To simulate this case, the upstream air flow is considered with 2 species (23.30% of O_2 and 76.69% of N_2). Behind the shock wave, the Park's chemical kinetics model[12] with 5 species O, N, NO, O_2, N_2 and 17 chemical reactions is used. O_2 and N_2 are each characterized by their proper vibrational temperature while NO is assumed to be in thermodynamic equilibrium with the translational temperature[13]. The Coupling Vibration-Dissociation (CVD) is taken into account according to the Park's model[12] with an average two temperature assumption. The coupling Vibration-Vibration(V-V) is given by Candler[14]. The influence of coupling V-V on the thermodynamic parameters is presented. A comparison with the DSMC results is also made.

The translational temperature isocontours are plotted in Fig. 7 for frozen flow. The maximum value of the ratio T/T_∞ behind the shock wave is 30% weaker than that predicted by the DSMC as in the case Mach 10. The pressure isolines are drawn in Fig. 8. The upper part represents the solution in which only CVD coupling is taken into account. The lower part is the solution obtained with simultaneous considerations of the CVD and V-V couplings. The thickness of the shock layer is visible and allows to appreciate the position and the intensity of the shock.

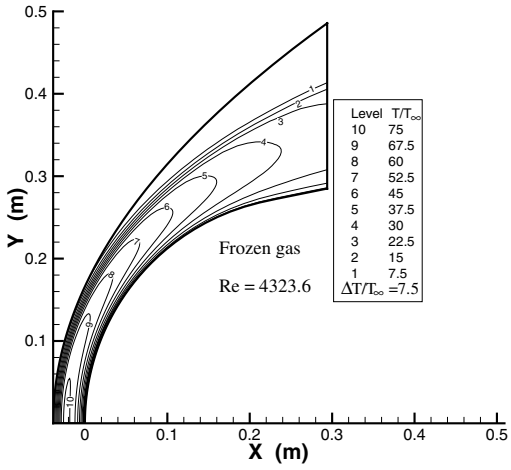

Figure 7. Isocontours of translational temperature; Mach 20.

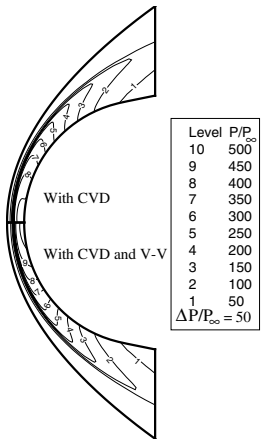

Figure 8. Influence of the coupling V-V on isopressions, Mach 20, $R_e = 4323.6$

TABLE 2. Various positions of the shock; SARA Mach 20

Mach 20	Frozen	with CVD	with V-V
X (m)	0,0350	0,0250	0,0225
$\delta = X/R\,(\%)$	6,9513	4,9652	4,4687

The influence of the nonequilibrium phenomena on the detachment of shock on the stagnation line is presented in table 2. Frozen case corresponds to a calculation without chemical reactions. The temperatures along the stagnation line are drawn in Fig. 9. The nonequilibrium vibrational of the molecules O_2 and N_2 leads to a distinct distribution of temperatures ($T_{v_{O_2}}, T_{v_{N_2}}$). This justifies the use of the model with three temperatures in spite of the strong Mach number, contrary to the use of a single temperature of vibration proposed by certain authors [15, 16]. Near the wall where temperature is low, one can note the influence of the V-V coupling. The difference between vibrational temperatures is more important without the V-V coupling, which leads to a transfer of a part of O_2 energy of vibration towards N_2, and confirms the tendency to bring closer the two temperatures of vibration. One notices an increase of the temperature $T_{v_{N_2}}$ behind the shock wave. The translational temperature T is about 13 000K behind the shock wave. This maximum is not sufficient to cause a significant ionization of gas under the upstream conditions used. Therefore, the ionization and electronic nonequilibrium are neglected.

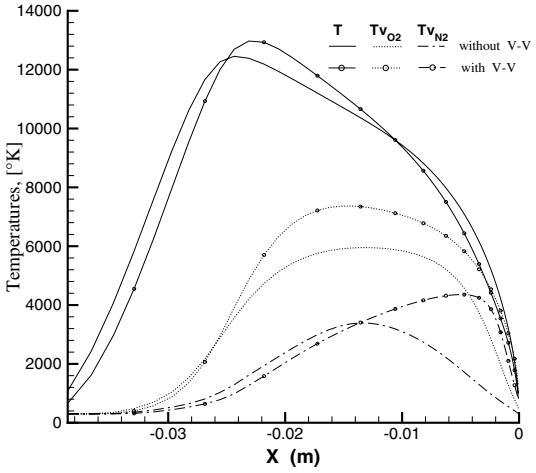

Figure 9. Temperatures distribution along the stagnation line, Mach 20, $R_e = 4323.6$.

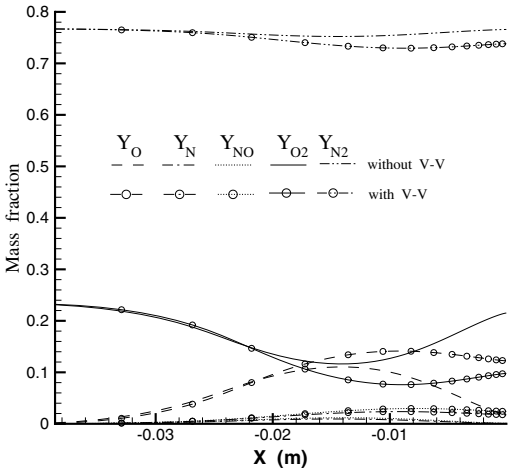

Figure 10. Mass fractions along the stagnation line, Mach 20, $R_e = 4323.6$.

The rise of temperature observed near the wall involves a greater dissociation of the nitrogen and oxygen molecules in the case of V-V coupling. The vibrational temperatures take part in the calculations of forward reaction rates. Fig. 10 shows a discrepancy of dissociation of approximately 52.38% for O_2 and 3.52% for N_2 at the stagnation point. This high dissociation of O_2 compared to N_2 can be explained by the fact that the O_2 molecules dissociate more quickly than N_2.

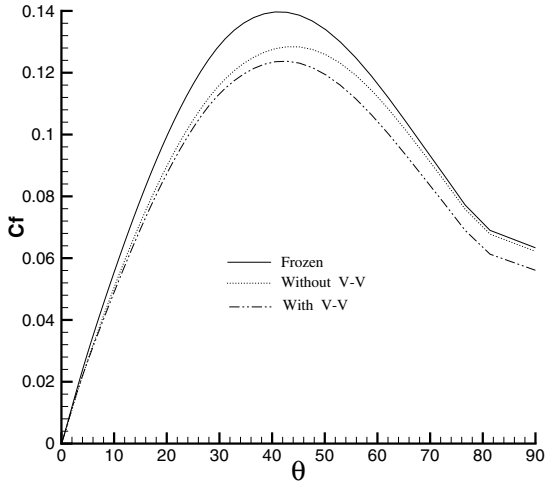

Figure 11. Friction coefficient, Mach 20, $R_e = 4323.6$.

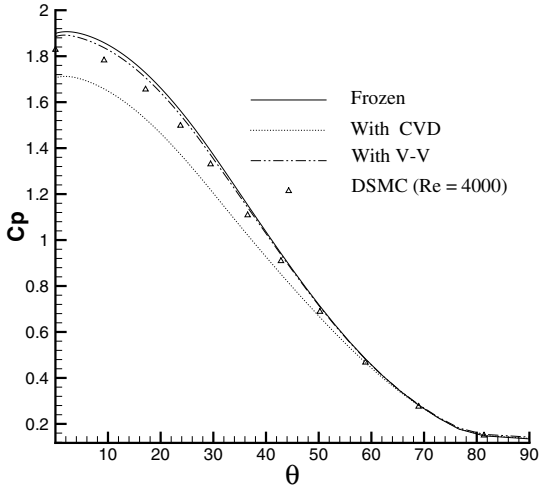

Figure 12. Comparison of C_p, Mach 20, $R_e = 4323.6$.

The evolution of coefficients C_f, C_p and C_h are given in Figs. 11, 12 and 13 as a function of the angle θ. The chemical reactions affect the thickness of the shock layer and one notes a decrease of the friction coefficient peak. The peak difference between calculations with coupling CVD and V-V is about 4.5%. The comparison of the pressure coefficient predicted between DSMC and this calculation is shown in Fig. 12. One notes a good agreement (2.12% of difference). In Fig. 13, the maximum value of the heat flux is located to the position $\theta = 0^o$. The importance of the dissociation reactions (endothermic) more accentuated in the case with V-V is remarkable on the wall heat flux. One observes a diminution of C_h of about 12.12% between the 2 cases. The difference of about 15.38% is also observed between the DSMC and this calculation at the stagnation point for frozen solution. This divergence may be explained by the initial conditions of simulation, because the conditions of $M_a = 20$ and $R_e = 4000$ can be obtained at altitude having different thermodynamic variables. Moreover, results presented are with $M_a = 20$ and $R_e = 4323.6$.

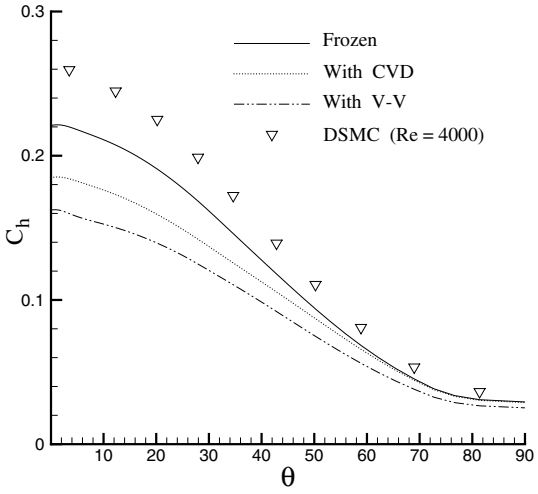

Figure 13. Comparision of coefficient C_h, Mach 20, $R_e = 4323.6$.

Case Mach 25

When the Mach number increases for the same altitude, the enthalpy increases and the ionized particles become important behind the shock wave. The air plasma surrounding re-entry vehicle may perturb the communications with the ground control, because plasma absorbs radio waves[19]. The objective of this section is to numerically study the influence of the ionized particles and the electronic excitation on the aerothermodynamics parameters. For that, an equation of electron-electronic relaxation and two additional species are taken into account (NO^+ and e^-). The choice of NO^+ is justified by the fact that the first energy of ionization (energy required to cause ionization) of NO is smallest. The flow are analysed thermally by using a model with four temperatures (T, $T_{v_{O_2}}$, $T_{v_{N_2}}$, T_e). The chemical kinetic model used for seven air species with 24 elementary reactions is proposed by Park[12].

The distribution of temperatures T, $T_{v_{N_2}}$ and T_e are represented in Fig. 14. The influence of the nonequilibrium

electronic excitation can be appreciated. One notes a decay of 12.25% of maximum of the translational temperature behind the shock wave cause by the translation - electronic coupling ($T - E$) which is defined here by Appleton and Bray[17]. The electronic - vibration coupling ($E - V$), according to the Landau - Teller[5] model, concerns only the nitrogen molecule in this work, its influence on the evolution of $T_{v_{N_2}}$ in the stagnation region is significant with a fall of the temperature ($\approx 23\%$). The skin friction coefficient decreases with the nonequilibrium effects as shown in Fig. 15. The wall heat flux is represented on Fig. 16. One notes an increase in heat flux of about 4.41% in $\theta = 0^o$ due to the electronic contribution. The taking into account of the thermochemical effects and their couplings brings a diminution of 19.04% of heat flux at the stagnation point between frozen and nonequilibrium calculation.

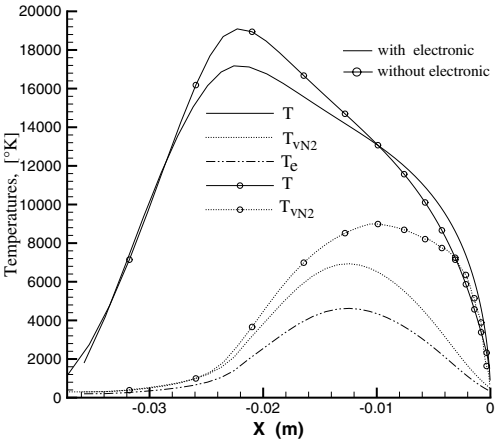

Figure 14. Temperatures distribution along the stagnation line, Mach 25, $R_e = 5404.5$.

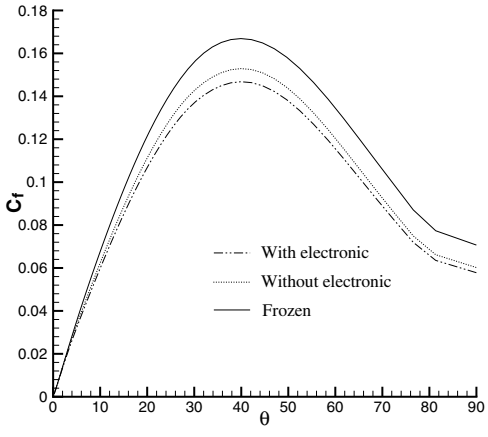

Figure 15. Friction coefficient, Mach 25, $R_e = 5404.5$.

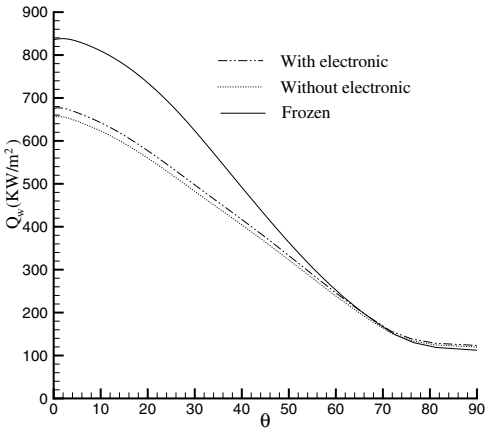

Figure 16. Wall heat flux, Mach 25, $R_e = 5404.5$.

5 Conclusion

This work is based on a series of numerical and fundamental studies of the flow around reentry satellite SARA in order to better predict the true importance for the thermal protection. The physical model accounted thermochemical nonequilibrium processes with a partially ionized gas. A robust 2D multiblock MUSCL-TVD finite volume scheme is used to solve the viscous flow at high Mach number. The correction of the speed of sound due to the presence of the electron temperature is also included. The various features of this complex flow are observed. The importance of the thermochemical phenomena on the aerothermodynamics parameters is pointed out. In the frozen case, the results show a good agreement for C_p and C_h with the DSMC calculations. The consideration of the thermochemical nonequilibrium effects allows to be more close to the physical reality within the flow and improves the prediction of results.

In a future work, the radiative phenomena will be included in the model.

References

[1] F. Sharipov, Braz. J. Phys. **33**, 398 (2003).

[2] C. Park and F. K. Milos, *Computational Equations for Radiating and Ablating Shock Layers*. AIAA paper 85-0247, January 1985.

[3] Lee Jong-Hun, *Basic Governing Equations for the Flight Regimes of Aeroassisted Orbital Transfer Vehicles.* Thermal Design of Aeroassisted Orbital Transfer Vehicles, H. F. Nelson, ed., Volume 96 of progress in Astronautics and Aeronautics, American Inst. of Aeronautics and Astronautics, Inc., c.1985, pp. 3-53.

[4] F. G. Blottner , M. Johnson and M. Ellis, *Chemically Reacting Viscous Flow Program for Multi-Component Gas Mixtures* Sandia Laboratories, Albuquerque, NM, Rept. Sc-RR-70-754, Dec. 1971.

[5] W. G. Vincenti and C. H. Kruger Jr., *Introduction to physical Gas Dynamics.* Krieger, FL, 1965.

[6] C. R. Wilke, Journal of Chemical Physics, **18**, 517 (1950).

[7] J. D. Ramsaw, and C. H. Chang, Plasma Chem Plasma process, **13**, 489 (1993).

[8] P. Roe, Jour. Comp. Phys. **43**, 357 (1983).

[9] Y. Burtschell, M. Cardoso and D.E Zeitoun, AIAA Journal, **39**, 2357(2001).

[10] G. Tchuen, *Modélisation et simulation numérique des écoulements à haute enthalpie: influence du déséquilibre électronique*. Thèse de Doctorat de l'Université de Provence - France, Novembre 2003.

[11] A. K. Hoffmann, T. S. Chiang, S. Siddiqui and M. Papadakis, *Fundamental Equations of Fluid Mechanics.* A Publication of Engineering Education System, Wichita, Kansas USA, 1996.

[12] C. Park, *Nonequilibrium Hypersonic Aerothermodynamics.* New York, Wiley 1990.

[13] G. Tchuen, Y. Burtschell and D.E Zeitoun, *Numerical prediction of weakly ionized high enthalpy flow in thermal nonequilirium.* AIAA Paper No. 2004-2462, 2004.

[14] G. V. Candler and R. W MacCormarck, Journal of Thermophysics and Heat Transfer, **5**, 266 (1991).

[15] P. A. Gnoffo, *A Code Calibration Program in Support of the Aeroassist Flight Experiment.* AIAA Paper No. 89-1673, 1989.

[16] C. Park, Journal of Thermophysics and Heat Transfer, **2**, 8 (1988).

[17] J. P. Appleton and K. N. C. Bray, J. Fluid Mech. **20**, 659 (1964).

[18] E. A. Masson and Monchick. The Journal of Chemical, **36**, 1622 (1962).

[19] J. Srinivasan and W. G. Vicenti, Phys. Fluids **18**, 1670 (1975).